Fabrication and Characterization of Nonplanar Microelectrode Array Circuits for Use in Arthroscopic Diagnosis of Cartilage Diseases

Eric Quenneville, Jean-Sébastien Binette, Martin Garon, Anne Légaré, Michel Meunier, and Michael D. Buschmann*

***Abstract*—A process to fabricate nonplanar microelectrode array circuits was developed and the microelectrodes were characterized. These platinum microelectrode arrays are for recording streaming potential signals generated during indentation of articular cartilage. The nonplanar substrate was produced by permanent deformation of a 7-in-diameter circular stainless-steel wafer to form 32 semi-spherical caps (radius of curvature $= 4.65$ mm and height $= 250$ μm) at the periphery. The wafer was covered with a 2.5-μm-thick layer of insulating polyimide. Standard microelectronic processes were applied to produce 32 circuits (60 mm long $\times$ 4 mm wide) with 37 exposed circular microelectrodes (diameter $= 100$ μm) centered over each semi-spherical cap. A 2.5-μm-thick photodefinable polyimide layer encapsulated the conducting lines. Capacitances between one microelectrode and either another microelectrode or the metallic substrate were 14.6 ± 2.0 and 34.4 ± 3.3 pF, respectively, at 100 Hz. The impedance of the microelectrodes in a 0.15 M saline bath (PBS) was 0.25 ± 0.08 MΩ while the crosstalk ($V_{induced}/V_{applied}$) between two microelectrodes was $0.20 \pm 0.11\%$, at 100 Hz. Indentation measurements were performed on articular cartilage *in vitro* showing streaming potentials that indicate electrode-tissue contact times and generation of streaming potentials.**

***Index Terms*—Cartilage electromechanics, microfabrication, Pt electrodes, streaming potentials.**

I. Introduction

ARTICULAR cartilage is the dense weight-bearing connective tissue covering the ends of bones in diarthroidal joints. It assures frictionless articulating joint surfaces during movement and distributes joint forces to the underlying subchondral bone [1]. Unfortunately, a variety of mechanical, chemical, and biological agents can damage articular cartilage [2]–[5]. Since adult cartilage is avascular, it has no access to normal wound repair processes and such injuries often slowly progress to diseases such as Osteoarthritis [6]. The lack of diagnostic tools capable of detecting cartilage degeneration in the early and potentially reversible stages of the disease, in addition to the absence of nerves in cartilage, may explain why diagnosis usually takes place at a symptomatic and essentially irreversible stage. At this point, few options other than joint replacement are available to the patient [7], [8]. In order to provide some specific indication of cartilage health versus disease, several instruments have been developed for *in vivo* cartilage diagnostics over the past decade [9]–[12]. Most of these diagnostic devices are based on measurements of cartilage stiffness (except [12] which uses electromechanical surface spectroscopy). In contrast, we have developed a diagnostic method using electrical (streaming) potential measurements obtained with an array of microelectrodes and have shown that this electromechanical technique bears certain advantages over purely mechanical tests [13]–[15].

Articular cartilage is characterized by solid and fluid phases, which represent 20%–35% and 65%–80% of the total mass, respectively. The solid phase is composed of a cross-linked collagen network ($\sim 60\%$), proteoglycans ($\sim 30\%$), in addition to other proteins and glycoproteins. The main proteoglycan in cartilage, aggrecan, is composed of negatively charged glycosaminoglycan chains attached to a central core protein. These molecules are entrapped within the collagen network via the formation of large (i.e., ~ 100 MD) aggregates of aggrecan and thereby generate an excess of mobile positive ions in the fluid phase to maintain electroneutrality [16]. Under equilibrium conditions, with no load or fluid flow, these opposite charges are symmetrically arranged so that no net macroscopic electric field exists. However, compression of the cartilage produces streaming potentials via the induction of a flow-generated displacement of the positively charged mobile counterions relative to the fixed, nonmobile, negatively charged proteoglycans [17]–[20]. Because they are related to the composition and the integrity of the extracellular matrix, streaming potentials created at the articular surface during compression have been shown to be sensitive indicators of cartilage health or stage of degeneration [21], [22].

The geometry of indentation testing is well suited for *in vivo* assessment of cartilage function through arthroscopic portals [23]. To record the streaming potentials during cartilage compression, a microelectrode array needs to be integrated into the surface of the indentor. The shape of the indentor, as well as the microelectrode distribution, should be optimized in order to facilitate cartilage evaluation. The use of a semi-spherical indentor presents some advantages over the other possible shapes. For example, the shape of the region of the indentor in contact with the

Manuscript received May 29, 2003; revised March 6, 2004. This work was supported in part by the NSERC Technology Partnerships Program, in part by the Canadian Arthritis Network, and in part by BioSyntech Canada Inc. *Asterisk indicates corresponding author.*

E. Quenneville, J.-S. Binette, and M. Garon are with the Institute of Biomedical Engineering and Department of Chemical Engineering, Ecole Polytechnique de Montreal, Montreal, QC H3C 3A7, Canada.

A. Légaré is with BioSyntech Canada Inc., Laval, QC H7V 4B3, Canada.

M. Meunier is with the Department of Engineering Physics and Materials Engineering, Ecole Polytechnique de Montreal, Montreal, QC H3C 3A7, Canada.

*M. D. Buschmann is with the Institute of Biomedical Engineering and Department of Chemical Engineering, Ecole Polytechnique de Montreal, P.O. 6079, station CV, Montreal, QC H3C 3A7, Canada (e-mail: michael.buschmann@polymtl.ca).

Digital Object Identifier 10.1109/TBME.2004.836522

cartilage is independent of the orientation of the indentor relative to the cartilage surface (this is not the case for a plane-ended indentor). This shape also minimizes generation of stress concentrations in the cartilage (e.g., such as those at the border of a plane-ended indentor) [24]. Also, the use of a high-density microelectrode array provides a great amount of information characterizing the manually applied indentation, since a distinct and sharp temporal response is produced by each electrode when it touches the tissue. Thus displacement and speed of the indentor as well as the indentor-cartilage contact area during cartilage compression can be monitored with high temporal resolution.

Macroscopic techniques are not well adapted for the production of high-density microelectrode arrays. Processes developed for microelectronics are more appropriate for such miniaturization requirements. However, these processes are currently only compatible with highly flat and smooth substrates. Since the microelectrode arrays need to lie on a semi-spherical surface, a deformable substrate needs to be embossed at different locations before the fabrication process begins. The main problem that arises here when using nonplanar substrates in microelectronic processes, in particular photolithography, is that a significant gap between the photomask and the substrate surface in some regions is unavoidable. This gap reduces the spatial resolution of the process due to optical diffraction. However, if the smallest dimension to be transferred from the photomask to the substrate is compatible with this loss of resolution, standard photolithographic processes on minimally deformed substrates can still be used.

In this paper, the fabrication process for microelectrode array circuits on nonplanar surfaces is presented along with their electrical characterization. This microelectrode array constitutes the sensing element of a minimally invasive hand-held arthroscopic device (Arthro-BST™, Bio Syntech Canada Inc., Laval, Canada) for the objective evaluation of articular cartilage structure and function for early diagnosis of arthritis and characterization of tissue repair.

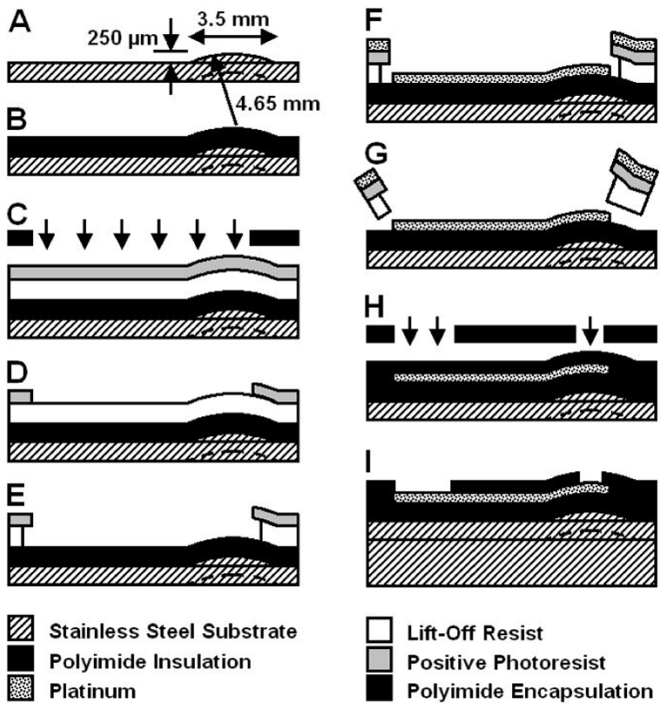

Fig. 1. Fabrication process for the microelectrode array circuits. (A) Semi-spherical caps were embossed in a stainless-steel substrate using a deformation press. (B) Layer of polyimide was spin-coated over the substrate. (C) Lift-off resist (LOR) and a positive resist were applied onto the polyimide layer and exposed to UV through a metallic layer mask. (D) Positive resist was developed and (E) LOR layer chemically etched. (F) The metallic layer (20 nm Ti followed by 180 nm Pt) was sputtered over the wafer, and (G) the unwanted metal was removed by lift-off. (H) Encapsulation layer of a photodefinable polyimide was spin-coated and exposed to UV through the encapsulation layer mask. (I) Encapsulation layer was developed and cured to expose 100-μm-diameter measurement points (37 per spherical cap in a hexagonally pattern + one reference electrode 1 cm away from the center of the cap) and the $0.8 \times 0.8\ \mathrm{mm}^2$ square pads for connection to the data acquisition system. The wafer containing multiple microelectrode circuits was then diced. The back of the spherical cap was filled with glue and the circuit was glued over a stainless-steel support.

II. Materials and Methods

A. Nonplanar Microelectrode Array Fabrication

A schematic of the fabrication process is shown in Fig. 1. Reagents were chemical grade unless otherwise noted. A stainless-steel foil type-316, $\sim$ 100 μm thick, (#69395, Precision Brand, Downers Grove, IL) machined as 7-in circular wafers was used as a substrate. They were deformed with a custom deformation press in order to create 32 semi-spherical caps ($\mathrm{curvature\ radius} = 4.65\ \mathrm{mm}$, $\mathrm{cap\ height} = 250\ \mu\mathrm{m}$, and $\mathrm{cap\ diameter} = 3.5\ \mathrm{mm}$) at the periphery of the wafer [Fig. 1(A)]. These spherical caps were made prior to the photolithographic process in order to avoid disruption of the thin film layers during embossment. The deformation profile of every spherical cap and the positioning of each cap on the wafer were critical since photolithography masks were aligned with the top of these caps with a lateral precision of $\pm 25\ \mu\mathrm{m}$.

The conducting metallic substrate was insulated with polyimide. The wafers were first thoroughly cleaned using heated solvents in the following order: Opticlear™ (NDIOE-101, DiaMed Lab Supply Inc., Mississauga, ON), acetone, isopropanol and water. They were then dried with a nitrogen gun and baked in a wafer oven at 200 °C for 30 min. A promoter (VM-651, HD MicroSystems, Parlin, NJ) of polyimide adhesion to the metallic substrate was spin-coated onto the wafer surface followed by a thin layer of polyimide (PI-2555, HD MicroSystems) [Fig. 1(B)]. The polyimide layer was cured in 40% RH lab air up to 300 °C followed by nitrogen up to 350 °C (2 °C/min) for 2 h. Thickness after cure was approximately 2.5 μm and surface roughness was less than 0.1 μm according to the profilometer (Dektak 3030, Veeco Instruments Inc., Woodbury, NY). Wafers were again cleaned and dried with the method described above.

A two-resist photolithographic process was applied prior to deposition of the metallic layer [Fig. 1(C)–(E)]. First, a 1-μm -thick layer of lift-off resist (LOR) (LOR-10 A, MicroChem Corp., Newton, MA) was spin-coated and prebaked at 140 °C for 35 min in order to dry the LOR film and to establish its development and undercut rate. Then, a second 1-μm-thick layer of positive photoresist (HPR-504, OCG Microelectronic Materials Inc., East Providence, RI) was spin-coated over the LOR layer and softbaked at 110 °C for 30 min in the wafer oven.

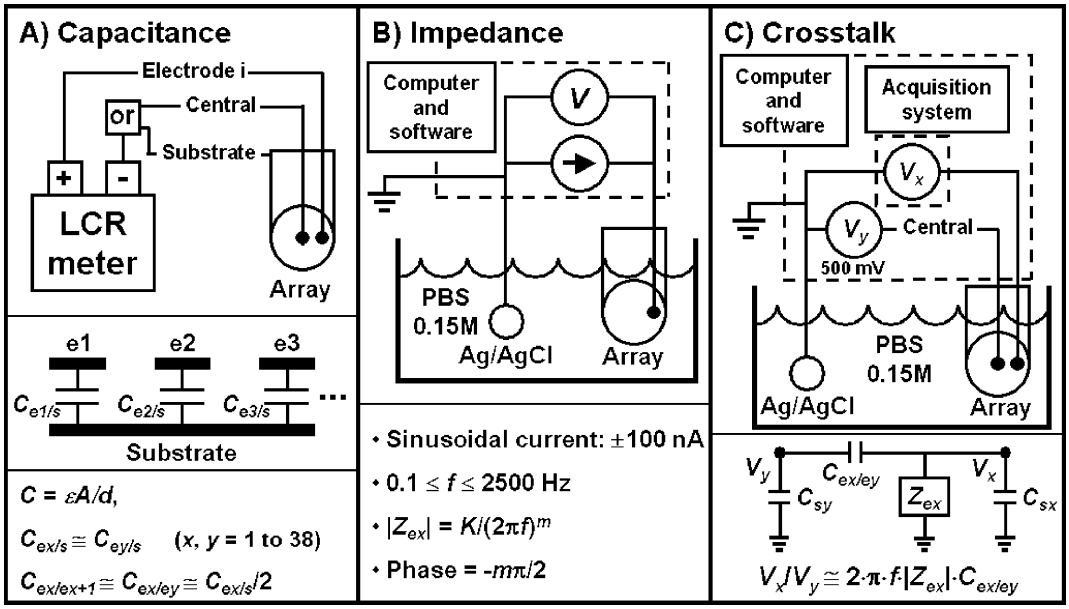

Fig. 2. Schematics of the setups used for the electrical characterization of the microelectrode arrays. (A) Capacitance between each microelectrode of the array and either the central microelectrode or the metallic substrate was measured using a LCR meter at 100 Hz. (B) Impedance of the microelectrodes to the passage of a 100-nA sinusoidal current was evaluated using an in-house computer-driven current source and voltmeter in the frequency range 0.1 to 2500 Hz. For the current to flow, the array was immersed along with a 1 cm^2 Ag/AgCl reference electrode in a 0.15 M PBS bath. The equations used in the impedance analysis are also shown. (C) Crosstalk level between electrodes was evaluated in the PBS bath by applying a 500-mV sinusoidal voltage between the Ag/AgCl reference electrode and the central microelectrode of the array and then by measuring the induced voltage signals between the reference electrode and each of the other microelectrodes. The simplified equivalent electrical circuit used to analyze the frequency behavior of the crosstalk is also shown [28].

This layer of photoresist was exposed [Fig. 1(C)] to UV light (G-line, $\lambda = 436$ nm) for 8 s through the metallic layer photomask (custom-design 7 in $\times 7$ in $\times 0.120$ in Sodalime AR Chrome produced by Image Technology, Palo Alto, CA) in the mask aligner (KSM MA 4, Karl Süss, Germany). During exposure, the mask was not in full soft-contact with the embossed wafer. Rather, only the tops of the 32 spherical caps were in soft-contact with the mask while the flat region of the wafer was separated from the mask by the height of the caps, i.e., 250 μm. The positive photoresist was developed for 40 s and then hard-baked at 125 °C for 30 min in the wafer oven. The patterned LOR layer was then removed by etching for 45 s in the chemical etchant solution (LDD-26 W, MicroChem Corp.) that also created a 1.5-μm undercut [Fig. 1(E)]. The remaining resists were then hardened at 120 °C for 30 min in the oven.

A platinum layer was sputtered over the wafer (magnetron sputtering) [Fig. 1(F)]. To improve the adhesion of this layer onto the polyimide coating, a 20-nm titanium layer was applied prior to the platinum layer. This single deposition process gave a 200-nm metallic layer composed of a 180-nm platinum layer on top of a 20-nm titanium layer. The unwanted regions of the metallic layer were removed by dissolving the resist layer in a liquid etchant for the LOR (Remover PG, MicroChem Corp.) in order to form the electrodes, the contact pads and the electrical conductors [Fig. 1(G)].

An encapsulating layer of photosensitive polyimide (PI-2723, HD Microsystems) was spin-coated over the wafer and then softbaked at 75 °C for 1 h in the wafer oven. The polyimide film was exposed to UV (G-line, $\lambda = 436$ nm) for 90 s through an encapsulation layer photomask (custom-design 7 in $\times 7$ in $\times 0.120$ in Sodalime AR Chrome produced by Image Technology) in the mask aligner [Fig. 1(H)]. Since this polyimide behaves like a negative working resist, the regions not exposed to UV were dissolved for 70 s in a polyimide developer followed by 2 min in a rinse solution (DE-8180 and RI-9180, HD MicroSystems). A 10-s (50:50, DE:RI) transition step between the developer and the rinse steps was also included. Wafers were gently dried with the nitrogen gun and then cured as for the first polyimide layer. The thickness of the cured layer was approximately 2.5 μm. Two types of patterns were transferred by photolithography onto the encapsulation layer: 1) the circular openings over the microelectrodes (diameter = 100 μm) and 2) the 0.8 mm $\times$ 0.8 mm square windows to create contact pads for signal acquisition.

Each of the 32 electrode circuits was then diced using scissors (a wafer saw or a die cutting technique could also be used). The back of the spherical cap was filled with glue (to increase its stiffness) and the circuit was glued onto a thick stainless-steel type-316 support using medical grade cyano-acrylate glue (#4011, Loctite, Mississauga, ON, Canada).

B. Electrical Characterization of the Microelectrode Array Circuits

The capacitance between each microelectrode x and either the stainless-steel substrate, $C_{ex/s}$, or the central microelectrode of the array, $C_{ex/ey}$, was measured using an LCR meter (4274 A, Hewlett-Packard) at 100 Hz [Fig. 2(A)]. These capacitances are mainly due to the conducting path from each microelectrode to its contact pad rather than to the microelectrode itself since the former has a much larger area than the latter.

The impedance of the microelectrodes was evaluated in the frequency range of 0.1–2500 Hz by immersing the array tip in a 0.15 M phosphate buffered saline solution (PBS) and injecting

a sinusoidal current of ± 100 nA through individual microelectrodes in the PBS and then out of solution via a 1 cm^2 Ag/AgCl electrode [Fig. 2(B)]. An equilibration time of 15 min was allowed prior to measuring the impedance using a custom bidirectional-output voltage controlled current source with buffered feedback described in [25, Fig. 4-37]. The amplitude, phase and total harmonic distortion (THD) of the impedance were calculated based on the fast Fourier transform (FFT) of 20 cycles of the signal and neglecting the impedance of the bathing solution and the reference electrode. The THD was calculated as the inverse ratio of the amplitude of fundamental frequency of the FFT to the sum of the amplitudes of the next seven harmonics. In the frequency range 10–2500 Hz, results were described by $|Z_{ex}| = K/(2\pi f)^m$ where $|Z_{ex}|$ is the impedance amplitude of the microelectrode x, K has the dimension of an ohmic impedance and, m is determined by the electrode material. This model also predicts a constant phase of $-m\pi/2$ [26].

Crosstalk between microelectrodes x and y is defined as the ratio of the induced potential on x divided by the potential applied on y. The level of crosstalk between microelectrodes was determined with the array circuit immersed in a PBS bathing solution and referenced to the Ag/AgCl electrode [Fig. 2(C)]. A 500-mV sinusoidal signal in the frequency range 0.1–2500 Hz was applied between the central microelectrode of the array [on its contact pad, i.e., V_y in Fig. 2(C)] and the reference electrode using an electrically isolated current source in the mV/V mode (model 2200, A-M Systems, Carlsborg, WA). The crosstalk signals induced on the other microelectrodes were then transferred to the acquisition system. A programmable electronic conditioning module was used for amplification ($30\times$) and filtering. Then signals were transferred to a data acquisition card (PCI-6031E, National Instrument) in a computer (Intel Pentium 4, 1.7 GHz) for digitization with 16-bit resolution at a sampling rate of 40 times the measured frequency [27]. The amplitude, phase and THD of the crosstalk signals were calculated as for the impedance. The frequency behavior of the crosstalk was analyzed with a simplified electrical equivalent circuit model described in [28] and presented here in Fig. 2(C). This model predicts the crosstalk to be

$$\frac{V_x}{V_y} = \frac{j \cdot 2\pi f \cdot C_{ex/ey}}{j \cdot 2\pi f \cdot (C_{ex/ey} + C_{sx}) + \frac{1}{Z_{ex}}}. \tag{1}$$

where V_x and V_y are, respectively, the induced and applied voltages, j is $\sqrt{-1}$, f is the frequency of the applied signal, $C_{ex/ey}$ is the capacitance between microelectrodes x and y, and Z_{ex} and C_{sx} are, respectively, the impedance and the shunt capacitance to the solution of the microelectrode recording the crosstalk signal. The value of shunt capacitance, C_{sx}, should be of the same order as $2C_{ex/ey}$ since the polyimide encapsulation layer has almost the same thickness as the insulation layer (see the discussion). With the measured values of the different parameters (see the results section), it can be assumed that $Z_{ex} \rightarrowtail 1/[j2\pi f \cdot (C_{ex/ey} + C_{sx})]$ for the frequency range under consideration and the ratio of the induced signal over the applied signal can be simplified to [28]

$$\frac{V_x}{V_y} \cong j \cdot 2\pi f \cdot Z_{ex} \cdot C_{ex/ey}. \tag{2}$$

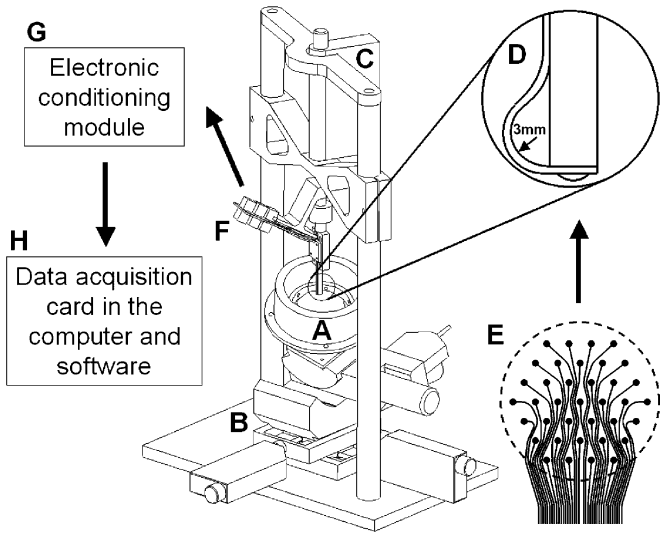

Fig. 3. Electromechanical testing apparatus for *in vitro* indentation of articular cartilage attached to bone. (A) Cartilage sample was fixed to the bottom of the testing chamber using screws. The test chamber was filled with buffered saline solution and (B) mounted on two linear and two angular actuators used to orient the cartilage surface perpendicularly to the compression axis of (C) the vertical linear actuator. (D) Microelectrode array circuit was glued onto a stainless-steel shaft such that (E) the microelectrode array on the spherical cap faces the cartilage surface. The streaming potentials measured by the array were acquired by (F) a high-impedance acquisition system composed of a conditioning card and (G) an electronic conditioning module. (H) Amplified signals were then transferred to a computer with custom software for data acquisition and analysis.

C. Electromechanical Indentation of Articular Cartilage

A block of articular cartilage (2 cm $\times$ 2 cm) attached to a thick layer of subchondral bone (1 cm) was harvested from the load-bearing region of a 2-year-old bovine shoulder and fixed to the base of a testing chamber [Fig. 3(A)] that was connected to a mechanical testing apparatus (Mach-1™ Mechanical Tester, Bio Syntech Canada Inc., Laval, Canada) (Fig. 3). The microelectrode array circuit [Fig. 3(E)] was mounted on the vertical linear actuator of the tester with the spherical cap facing down [Fig. 3(D)]. The testing chamber was filled with 0.15 M PBS solution and the cartilage surface was oriented perpendicularly to the compression axis using the angular actuators [Fig. 3(B)], so that the spherical cap would indent the cartilage surface perpendicularly with the central electrode of the array touching the cartilage surface first. Five ramp-release indentations were then applied using a compression amplitude of 300 μm and speed of 100 μm/s followed by a 2-s wait phase (plateau) and a release at -1000 μm/s. The indentations were performed at the same position on the sample with a rest time of 1 h 30 min between compressions. The streaming potential signals measured with the microelectrode array were recorded by a high input impedance acquisition system [Fig. 3(F)–(H)]. The electrical potential signals were first transferred to a conditioning card designed to buffer signals with high input impedance followers (OPA4350, Burr-Brown, Tucson, AZ). Signals were then transferred from the conditioning card to the programmable electronic conditioning module then to the data acquisition card of the computer (as for the crosstalk measurements). The acquisition rate was 600 Hz/channel and a 100-Hz low-pass filter was used [27]. Each signal was referenced to the potential of a 38th

TABLE I
AVERAGE VALUES AND STANDARD DEVIATIONS ($n = 100$) FOR THE ELECTRICAL CHARACTERISTICS OF THE MICROELECTRODES AT 100 HZ

	Capacitance [a]		Impedance [b]			Crosstalk [b]		
	Central Electrode (pF)	Substrate (pF)	Amplitude (MΩ)	Phase (°)	THD (%)	Amplitude (%)	Phase (°)	THD (%)
Average	14.6 [17.2]	34.4 [28]	0.25 [0.24]	-69 [-66]	0.71	0.20 [0.23]	50 [24]	8
St.Dev.	2.0	3.3	0.08	6	0.76	0.11	5.5	5

The values predicted by the different models for the capacitance (Fig. 2A), impedance (Fig. 2B), and crosstalk (Fig. 2C) are presented in square brackets.
[a] Capacitances between one electrode and either the central microelectrode of the array or the metallic substrate.
[b] Values obtained when the central microelectrode of the array is injected with 500 mV.

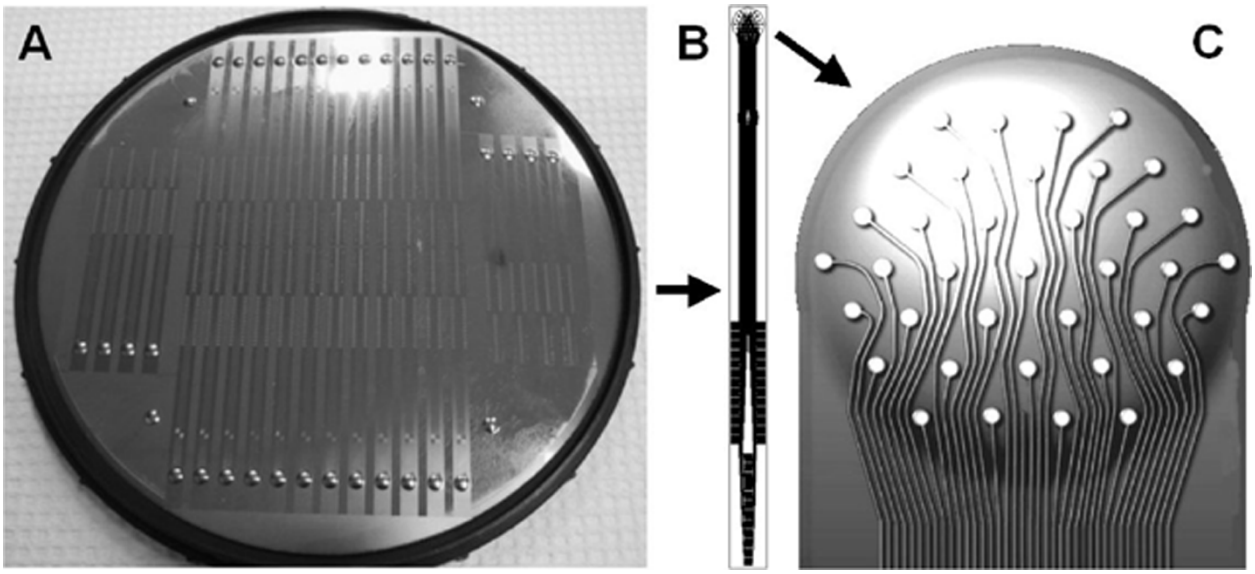

Fig. 4. (A) Completed microelectrode array circuits ($n = 32$) on one wafer prior to dicing. (B) Schematic of the metallic layer of one completed microelectrode array. (C) Schematic of the 37 microelectrodes over the semi-spherical cap at one end of the circuit.

platinum microelectrode with the same dimensions as the other, but located 1 cm away from the center of the spherical cap. This differential referencing minimized noise pick-up, microphonic effects, as well as the electrical drift of the platinum microelectrodes in the saline bath. The contact between the microelectrode array circuit and the conditioning card was achieved with a custom 15 cm long polyimide-copper flexible circuit (from Flexible Circuit Technology Inc., St. Paul, MN).

III. RESULTS

A. Nonplanar Microelectrode Array Fabrication

Thirty-two microelectrode array circuits on a 7-in stainless-steel wafer are shown in Fig. 4(A). The arrays were fabricated on top of semi-spherical caps embossed at the periphery of the metallic wafer at the beginning of the process. All of the thin film processing steps were completed for the wafer shown in Fig. 4(A) and this wafer is ready for dicing. A schematic of the metallic layer of one completed microelectrode array circuit is presented in Fig. 4(B). The 38 contact pads are located on three columns at the bottom of the figure. The microelectrode array on the semi-spherical cap is located at the top end of the circuit. A thin platinum-conducting line with a 25-μm width links each microelectrode to its corresponding contact pad. A schematic enlargement of the top end of the circuit is presented in Fig. 4(C) where 37 microelectrodes are shown over the semi-spherical cap. The distance between any two adjacent microelectrodes (500 μm) is five times their diameter (100 μm). A 38th microelectrode, with the same diameter and used for referencing the other microelectrodes, is located 1 cm away from the center of the spherical cap (not shown).

B. Electrical Characterization of the Microelectrode Circuits

The capacitance at 100 Hz between any two microelectrodes and between a microelectrode and the substrate were 14.6 ± 2.0 and 34.4 ± 3.3 pF, respectively ($n = 100$) (Table I). The impedance of a 7.9×10^{-5} cm^2 platinum microelectrode was 0.25 ± 0.08 MΩ at 100 Hz ($n = 100$) (Table I). Microelectrode impedance varied with frequency from 10 to 2500 Hz similarly to that predicted by the model [Fig. 5(A)] [26]. The best fit of the experimental data to the model over this frequency range was obtained with $K = 26.4$ MΩ and $m = 0.73$. When the frequency was below 10 Hz, the model overestimated the electrode impedance. The crosstalk measured at 100 Hz was $0.20 \pm 0.11\%$ ($n = 100$) (Table I). The variation of the crosstalk with frequency, at frequencies below 200 Hz, was close to that predicted by the simplified equivalent circuit model described in the method [Fig. 5(B)] [28]. At higher frequencies greater than 200 Hz the discrepancy between measured crosstalk values and the model became significant.

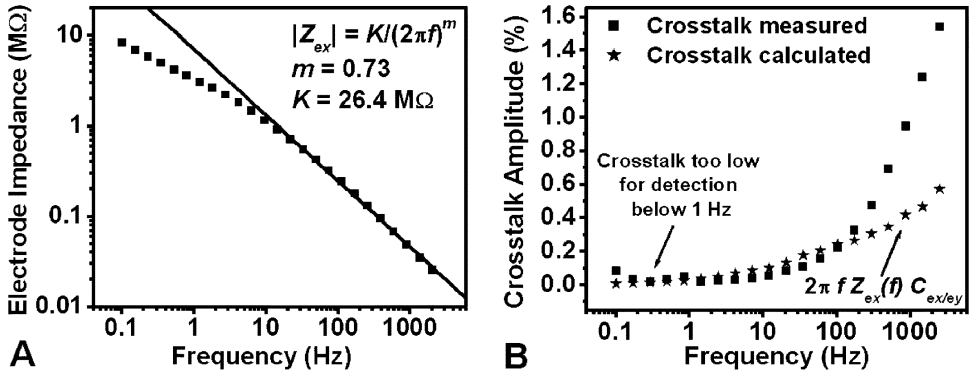

Fig. 5. (A) Representative behavior of microelectrode impedance versus frequency. Impedance above 10 Hz was fit to $|Z_{ex}| = K/(2\pi f)^m$ to obtain $m = 0.73$ and $K = 26.4\ \mathrm{M}\Omega$. (B) Representative behavior of the crosstalk amplitude versus frequency measured on an adjacent electrode when a 500-mV sinusoidal signal was applied to the central microelectrode of the array. The black stars represent the calculated crosstalk values based on the simplified equivalent circuit model, i.e., $V_x/V_y \cong 2 \cdot \pi \cdot f \cdot |Z_{ex}(f)| \cdot C_{ex/ey}$, with the impedance of (A) and the average value of Table I for $C_{ex/ey}$.

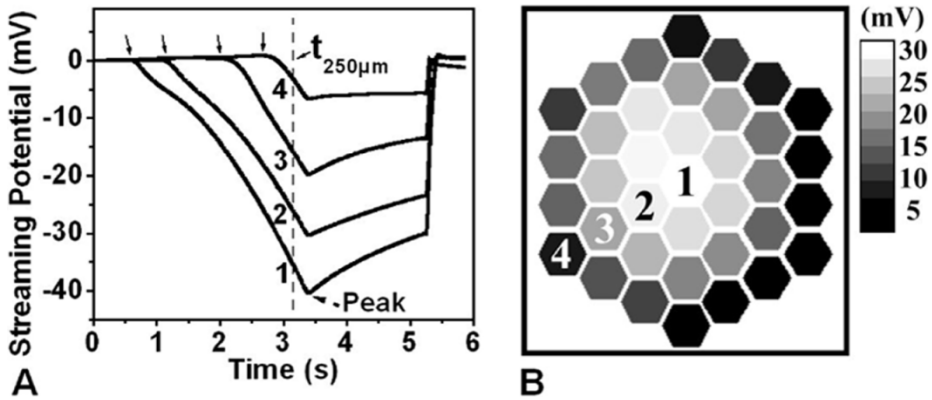

Fig. 6. (A) Representative streaming potentials measured during indentation of articular cartilage attached to bone with the microelectrode array on the semi-spherical cap. A 300-μm compression at 100 μm/s was applied followed by a 2-s wait phase (plateau) and then a release at -1000 μm/s. Four representative streaming potential signals (corresponding to the numbered electrodes in B) show the initial time of contact (arrows), followed by increasing negative potentials up until the peak where compression stopped. Partial relaxation occurred during the plateau followed by a quick return to ground at release. (B) The hexagonal electrode pattern is shown in gray scale where lighter tones indicate higher absolute potentials at the time corresponding to a 250-μm compression of the central electrode (vertical dotted line in A).

C. Electromechanical Indentation of Articular Cartilage

The spatial distribution and time-dependence of the electrical potentials measured by the microelectrode array on the spherically shaped tip during indentation of articular cartilage are shown in Fig. 6(A). After perpendicular alignment and determination of the height of contact with the articular surface, indentation at constant velocity resulted in an increasingly negative potential once the electrode contacts the articular surface [arrows in Fig. 6(A)]. When interpreting these results, it is important to note that streaming potential is approximately proportional to interstitial fluid pressure [27]. Given the semi-spherical geometry of the indentor tip, each microelectrode contacted the cartilage surface at a different time with the central microelectrode contacting cartilage first. Knowing the curvature of the indentor and the contact time of each signal, it was possible to deduce the point of contact of the indentor with the cartilage surface and to calculate the speed at which the cartilage was compressed. For all the microelectrodes, the highest streaming potential amplitude was measured at a displacement of 300 μm corresponding to the end of the applied compression. During the subsequent 2-s wait phase, or plateau, streaming potentials decreased due to fluid flow-related relaxation and dissipation of interstitial fluid pressure. The indentor was then released and all the potentials returned to zero. For the five successive indentations, the maximum streaming potential amplitudes were -41.5, -41.0, -40.5, -39.9 and -39.5 mV, respectively, and the radial profiles were almost identical (not shown). These results were not averaged. A snapshot of the two-dimensional (2-D) potential profile across the hexagonal array at the time when the central electrode was at a 250-μm depth shows the 2-D distribution of potentials with higher values (and, therefore, pressures) within the central region that decrease toward the periphery [Fig. 6(B)].

IV. Discussion

The deformability of the composite substrate (a polyimide thin film over a metallic foil) constitutes a major advantage over rigid semi-conductor wafers commonly used in microfabrication. In particular, this deformability allows the substrate to be embossed to create semi-spherical caps for use in cartilage diagnosis via electromechanical indentation. Also, it allows the resulting circuits to be deformed in order to conform to almost any shape of the solid support. We have verified that the circuit can be permanently bent to a radius of curvature down to 3 mm

(perpendicularly to the metallic traces) without thin film fracture or variations in the recorded potentials.

The most obvious difficulty when using standard microfabrication processes on nonplanar surfaces results from optical diffraction of the UV light by the photomask during photolithography. In our case, the mask is placed about 250 μm above the lower nonembossed flat regions of the substrate during the soft-contact with the top of the semi-spherical caps. Thus, optical diffraction increases the area exposed to UV in the resist layer to be slightly larger than that of the clear area on the photomask. In order to design the photomask, it is necessary to know the minimal pattern dimension that can be resolved with this gap. Based on Rayleigh's criterion, in the approximation of Fraunhofer diffraction for multiple linear gratings, the minimal pattern dimension that can be resolved with this gap is about 15 μm (i.e $\sim 1.4 \cdot (\lambda \cdot \text{gap})^{1/2}$) [29]. Using this theoretical dimension as a reference, we decided on 25 μm as the minimal pattern dimension on the photomask. For multiple linear gratings of 25 μm spaced by 250 μm from the substrate, it can be calculated that only 3% of the total illumination will exceed the pattern boundaries defined by the photomask. If the exposure time is controlled to avoid overexposure, the resist can still be patterned with the original mask layout, but diffraction will result in poor wall definition [30]. This situation will compromise any attempt to use standard lift-off processes.

By using two resists (a standard positive photoresist over a chemically etched resist) instead of a single resist, the lift-off process can be realized successfully (Fig. 7). With a single resist [Fig. 7(A)], diffraction will cause a significant thickness variation in the resist walls and the sputtered metallic thin film will form a continuous layer over the whole wafer. This will reduce access of the solvent to the resist layer and compromise the removal of unwanted metal. A second underlying resist, that can be chemically etched, solves this problem of the resist wall profile [Fig. 7(b)]. No extra lithographic step is needed to define the underlying resist, since it is self-aligned with the first resist layer. The etching time is however optimized to completely remove the resist where the metallic layer is needed and to create an undercut that is compatible with the lift-off process. Note that excessive etching time will cause the top resist layer (thinner at the edge) to collapse on the substrate and the result will be equivalent to the single resist case. Once the metallic layer is sputtered over the wafer, the unwanted metal is completely removed by dissolving the bottom resist in its associated solvent.

Since the thickness of the polyimide isolation layer is very small, a capacitance between each microelectrode trace and the metallic substrate can be significant and must be measured [Fig. 2(A)]. Using the relative dielectric constant for the polyimide [33], 3.4, the average capacitor surface, 2.3 mm^2, and the average polyimide layer thickness, 2.5 μm, the average capacitance of the microelectrode traces with the substrate, $C_{ex/s}$, should be around 28 pF. This estimate is close to the value shown in Table I of 34.4 ± 3.3 pF. Thickness variations in the polyimide layer, particularly at the top of the semi-spherical cap where it is thinner, could be responsible for the higher measured values. The capacitance measured between each microelectrode and the central microelectrode of the array results from the series combination of the capacitance between each microelectrode and the substrate, i.e., $C_{ex/ey} = C_{ex/s} \cdot C_{ey/s}/(C_{ex/s}+C_{ey/s}) \approx C_{ex/s}/2 = 17.2$ pF, also close to the measured value, 14.6 ± 2.0 pF (Table I). Notably, the direct capacitance between adjacent microelectrode traces on the polyimide layer is negligible due to the thinness of the metallic layer. Since the Young's Modulus of the polyimide layer is very high (~ 2.7 GPa), a variation of the capacitance due the contact pressure observed during a measurement (1-20 MPa) will be also negligible.

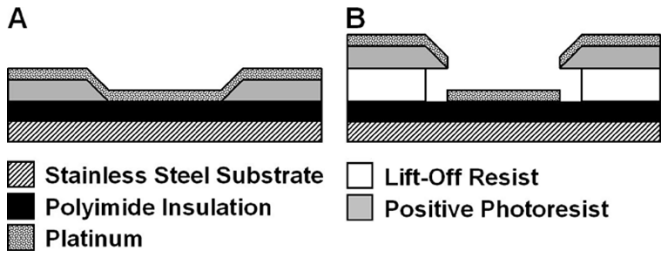

Fig. 7. A standard lift-off process compared to a LOR lift-off process for the lithography of the metallic layer. (A) In a standard lift-off process, diffraction on the photomask (spaced by a 250-μm gap) will cause a significant thickness variation in the resist walls, so that the sputtered metallic thin film will form a continuous layer over the whole wafer and the unwanted metal will be difficult to remove. (B) The use of a second underlying resist that can be chemically etched solves the problem of the resist wall profile. The underlying resist is self-aligned with the top photoresist layer. The etching time is optimized to completely remove the resist where the metallic layer is needed and to create an undercut that will facilitate the lift-off of the unwanted metal.

The reduction of the microelectrode impedance with the frequency can be well described by $K/(2\pi f)^m$, in the frequency range from 10 to 2500 Hz, and is similar to what has been previously reported in the literature [26], [31]. This model was used by de Boer *et al.* to fit impedance measurements on small flat platinum electrodes over the same frequency range [26]. This group found $m = 0.75$ and KA values in the range 1.0 to 1.8 $\text{k}\Omega\cdot\text{cm}^2$, where, A, stands for the electrode active area ($A = 5\times10^{-4}\ \text{cm}^2$). The best fit of this model to our impedance measurements is obtained using $m = 0.73$ and $K = 26.4\ \text{M}\Omega$. For our $7.9\times10^{-5}\ \text{cm}^2$ microelectrodes this corresponds to $KA = 2.1\ \text{k}\Omega\cdot\text{cm}^2$. The close match of the m values is an indication that the electrode material behaves as expected for a platinum electrode while our value found for KA is slightly higher than the reported range, possibly due to the smoothness of our thin film microelectrodes compared to the macroscopically produced electrodes of [26]. With our m value, the predicted phase is $-66°$ while the measured value was $-69 \pm 6°$ (Table I).

Crosstalk is observed between microelectrodes, but its effect on the recorded signals during cartilage indentation is negligible. This is true even for signals with amplitudes at least two times higher (500 mV) than any typical streaming potential measured during cartilage compression. At 100 Hz, the averaged crosstalk amplitude was $0.20 \pm 0.11\%$ (see Table I). This crosstalk level is compatible with what can be found using the simple equivalent circuit model for crosstalk described in the methods section. With the capacitance and the impedance values of Table I, the predicted crosstalk is 0.23% (i.e., $2 \cdot \pi \cdot 100\ \text{Hz} \cdot 0.25\ \text{M}\Omega \cdot 14.6$ pF). The simplified model describes the general frequency behavior of the crosstalk, but underestimates its value at high frequency. This may be due to the contribution of different sources of capacitance, neglected in the

model, that become more important at higher frequencies (e.g., the shunt capacitance with the solution, capacitance between conductors in the flexible interconnection circuit or in the acquisition system). In the case where the same electrical signal is simultaneously recorded on 36 of the 37 microelectrodes of the array, the crosstalk signal on the 37th microelectrode could be as high as $36 \times 0.23\% = 8.3\%$ at 100 Hz. At first sight, this perturbation level may seem unacceptable [32], however, for the particular application of measuring streaming potentials of cartilage, much of the frequency content of the signal is below 30 Hz. In this frequency range, the crosstalk induced by one electrode is lower than 0.1% [Fig. 5(B)], leading to less than 3.6% crosstalk for the total microelectrode array. Moreover, the streaming potentials are not all of high amplitude simultaneously over the spherical cap and the small signals measured by almost half of the microelectrodes will cause only a minimal crosstalk (Fig. 6). For these reasons, crosstalk is normally lower than 2% when measuring streaming potential signals with these circuits.

The indentation measurements on cartilage were done in order to verify that the streaming potentials measured by the microelectrode array are compatible with the known electromechanical properties of articular cartilage. The indentation of articular cartilage with a microelectrode array bearing spherical tip showed a spatial distribution and time-dependence of electrical potentials that indicate: 1) the contact of each electrode with the articular surface; 2) the electromechanical induction of streaming potentials corresponding to the expected rise of interstitial fluid pressure; 3) fluid flow-related relaxation; and 4) the release of indentor contact [Fig. 6(A)]. Although there is no published theoretical description of the poroelastic electromechanical behavior of cartilage during spherical indentation, the measured potential distribution and its time evolution during the indentation can be surmised from models and experiments performed in unconfined compression [27], [33]. The measured streaming potentials are expected to be negative due to the negatively charged proteoglycan entrapped in the collagen network. Linear infinitesimal models [17]–[19], [34] suggest proportionality between the local streaming potential and the local pore pressure. Because cartilage is more compressed near the center of the indenter, the local pore pressure, as well as the potential, is higher in magnitude [Fig. 6(A)–(B)]. At the periphery, the pressure is almost zero and the measured potentials are also very small. The reduction in the potential amplitude observed for all microelectrodes during the 2-s plateau is also expected via the poroelastic model due to the reduction of the pore pressure caused by water flowing out of the sample. In addition, each microelectrode of the array measured a different potential signal in terms of amplitude and/or noise confirming what was found by direct probing on the contact pads of the microelectrode array circuit that there was no open- or short-circuits. The reproducibility of the measured streaming potential signals was also very good for all microelectrodes during the five indentations. The small reduction in the maximum potential recorded by the central electrode is correlated with the time at which the experiment was done. This reduction may be due to a slow degradation or the cartilage during the 6-h experiment.

Biocompatibility of the materials constituting the microelectrode array is an important aspect, even though they will only be temporarily in contact with body tissues and fluids. Materials that could possibly enter in contact with body tissues (stainless-steel type-316, polyimide, platinum and medical grade glue) have been selected since they are known to be biocompatible. Stainless steel type-316 is an alloy used extensively in the fabrication of a broad spectrum of medical grade tools. Studies of commercially available polyimide used as substrates for cochlear prostheses have also shown good biocompatibility after long-term implantation [35], [36]. An *in vitro* study of five types of polyimide demonstrated that these materials do not elicit any cytotoxic response, and induce little haemolysis and only a moderate degree of coagulation (97–98% of normal for Kapton™) making polyimides an attractive candidate as biosensor encapsulants [37]. Platinum, a noble metal, is generally reported as nontoxic [38] while the medical grade cyano-acrylate glue (Loctite, 4011) also complies with the Loctite ISO-10 993 Biocompatibility test program.

V. Conclusion

Microelectrode array circuits that can be used for the detection of compression-induced streaming potentials on articular cartilage were developed and characterized. An array of 37 circular platinum microelectrodes with exposed diameters of 100 μm was produced on a minimally deformed semi-spherical surface using standard microelectronic processes. The loss of resolution in the lithographic steps, caused by the gap between the mask and the wafer (250 μm), can be tolerated due to the relatively large minimal pattern dimension in the circuit (25 μm) and the use of two layers of photoresist. The composite substrate formed by the application of a polyimide layer over thin stainless-steel substrate allow the circuit to be deformed and shaped to access different portions of the articular cartilage surface in a joint. The electrical characterization of the microelectrodes, determined by recording the streaming potential distribution during cartilage indentation and by measuring electrode capacitance, impedance and crosstalk, demonstrated that the circuits could be used for accurate and reliable assessment of cartilage properties.

Acknowledgment

Authors want to thank M. Ouellet for his help with the electromechanical measurements, and the technical staff of the microfabrication laboratory of the Department of Engineering Physics of Ecole Polytechnique de Montreal for their assistance with the microelectrode circuit fabrication.

References

[1] M. D. Buckwalter and H. J. Mankin, "Articular cartilage: Part I," *J. Bone Joint Surg*, vol. 79A, pp. 600–611, Apr. 1997.

[2] A. P. Newman, "Articular cartilage repair," *Amer. J. Sports Med.*, vol. 26, pp. 309–324, Feb. 1998.

[3] M. Thibault, A. R. Poole, and M. D. Buschmann, "Cyclic compression of cartilage/bone explants *in vitro* leads to physical weakening, mechanical breakdown of collagen and release of matrix fragments," *J. Orthop. Res.*, vol. 20, pp. 1266–1274, June 2002.

[4] H. J. Mankin, "The response of articular cartilage to mechanical injury," *J. Bone Jont Surg. Amer.*, vol. 64, pp. 460–466, Mar. 1982.
[5] C. G. Armstrong and V. C. Mow, "Variations in the intrinsic mechanical properties of human articular cartilage with age, degeneration, and water content," *J. Bone Joint Surg*, vol. 64A, pp. 88–94, Jan. 1982.
[6] J. A. Buckwalter, "Articular cartilage: Injuries and potential for healing," *J. Orthop. Sports Phys. Therapy*, vol. 28, pp. 192–202, Apr. 1998.
[7] J. A. Buckwalter and S. Lohmander, "Operative treatment of osteoarthrosis: Current practice and future development," *J. Bone Jont Surg. Amer.*, vol. 76, pp. 1405–1418, Sept. 1994.
[8] E. Lexer, "Substitution of whole or half joints from freshly amputated extremities by free plastic operation," *Surg. Gynecol. Obstetrics*, vol. 6, pp. 601–609, 1908.
[9] T. Lyyra, J. Jurvelin, P. Pitkänen, U. Väätäinen, and I. Kiviranta, "Indentation instrument for the measurement of cartilage stiffness under arthroscopic control," *Med. Eng. Phys.*, vol. 17, pp. 395–399, 1995.
[10] R. C. Appleyard, M. V. Swain, S. Khanna, and G. A. C. Murell, "The accuracy and reliability of a novel handheld dynamic indentation probe for analysing articular cartilage," *Phys. Med. Biol.*, vol. 46, pp. 541–550, 2001.
[11] M. S. Laasanen, J. Töyräs, J. Hirvonen, S. Saarakkala, R. K. Korhonen, M. T. Nieminen, I. Kiviranta, and J. S. Jurvelin, "Novel mechano-acoustic technique and instrument for diagnostic of cartilage degeneration," *Physiol. Meas.*, vol. 23, pp. 491–503, 2002.
[12] S. I. Berkenblit, E. H. Frank, E. P. Salant, and A. J. Grodzinsky, "Non-destructive detection of cartilage degeneration using electromechanical surface spectroscopy," *J. Biomech. Eng.*, vol. 116, pp. 384–392, 1994.
[13] E. Quenneville, M. Garon, A. Légaré, M. Hurtig, and M. D. Buschmann, "Diagnostic mapping of bovine and equine articular cartilage with a new arthroscopic device," presented at the *Can. Arthritis Network Meeting*, Calgary, AB, Canada, Sept. 2002.
[14] M. Garon, A. Légaré, E. Quenneville, and M. D. Buschmann, "Streaming potential based arthroscopic instrument distinguishes site-specific properties of equine articular cartilage," in *Proc. Orthopaedic Research Society Meeting*, vol. 28, New Orleans, LA, Feb. 2003, Paper 255.
[15] E. Quenneville, M. Garon, A. Légaré, and M. D. Buschmann, "Load and streaming potential responses of articular cartilage as a function of compression speed during indentation," in *Proc. Orthopaedic Research Society Meeting*, vol. 28, New Orleans, LA, Feb. 2003, Paper 659.
[16] A. Maroudas and H. Evans, "A study of ionic equilibria in cartilage," *Connect. Tissue Res.*, vol. 1, pp. 69–77, 1972.
[17] W. M. Lai, J. S. Hou, and V. C. Mow, "A triphasic theory for swelling and deformation behavior of articular cartilage," *J. Biomech. Eng.*, vol. 113, pp. 245–258, 1991.
[18] E. H. Frank and A. J. Grodzinsky, "Cartilage electromechanics-I. Electrokinetic transduction and the effects of electrolyte pH and ionic strength," *J. Biomech.*, vol. 20, pp. 615–627, June 1987.
[19] ——, "Cartilage electromechanics-II. A continuum model of cartilage electrokinetics and correlation with experiments," *J. Biomech.*, vol. 20, pp. 629–639, June 1987.
[20] M. D. Buschmann and A. J. Grodzinsky, "A molecular model of proteoglycan-associated electrostatic forces in cartilage mechanics," *J. Biomech. Eng.*, vol. 117, pp. 179–192, Feb. 1995.
[21] E. H. Frank, A. J. Grodzinsky, T. J. Koob, and D. R. Eyre, "Streaming potentials: A sensitive index of enzymatic degradation in articular cartilage," *J. Orthop. Res.*, vol. 5, pp. 497–508, Apr. 1987.
[22] A. Légaré, M. Garon, R. Guardo, P. Savard, A. R. Poole, and M. D. Buschmann, "Detection and analysis of cartilage degeneration by spatially resolved streaming potentials in articular cartilage," *J. Orthop. Res.*, vol. 20, pp. 208–215, 2002.
[23] W. C. Hayes, L. M. Keer, G. Herrmann, and L. F. Mockros, "A mathematical analysis for indentation tests of articular cartilage," *J. Biomech.*, vol. 5, pp. 541–551, 1972.
[24] J. K. Suh and R. L. Spilker, "Indentation analysis of biphasic articular cartilage: Nonlinear phenomena under finite deformation," *J. Biomech. Eng.*, vol. 116, pp. 1–9, 1994.
[25] W. G. Jung, "Voltage regulators, references, and power supplies using op amps," in *IC OP-AMP Cookbook*, 3rd ed. Indianapolis: Howard W. Sams & Co. Inc., 1990, pp. 169–218.
[26] R. W. de Boer and A. van Oosterom, "Electrical properties of platinum electrodes: Impedance measurements and time-domain analysis," *Med. Biol. Eng. Comput.*, vol. 16, pp. 1–10, 1978.
[27] M. Garon, A. Légaré, R. Guardo, P. Savard, and M. D. Buschmann, "Streaming potentials maps are spatially resolved indicators of amplitude, frequency and ionic strength dependant responses of articular cartilage to load," *J. Biomech.*, vol. 35, pp. 207–216, 2002.
[28] T. Akin, B. Ziaie, S. A. Nikles, and K. Najafi, "Modular micromachined high-density connector system for biomedical applications," *IEEE Trans. Biomed. Eng.*, vol. 46, pp. 471–480, Apr. 1999.
[29] W. C. Elmore and M. A. Heald, *Physics of Waves*. New York: Dover /McGraw-Hill, 1969, pp. 351–374.
[30] S. P. Murarka and M. C. Peckerar, *Electronic Materials Science and Technology*. Boston, MA: Academic, 1989, p. 622.
[31] A. R. Varlan and W. Sansen, "Characterization of planar electrodes realized in planar microelectronic technology," *Med. Biol. Eng. Comput.*, vol. 34, pp. 308–312, 1996.
[32] O. J. Prohaska, F. Olcaytug, P. Pfundner, and H. Dragaun, "Thin film multiple electrode probes: Possibilities and limitations," *IEEE Trans. Biomed. Eng.*, vol. BME-33, Feb. 1986.
[33] J. Soulhat, M. D. Buschmann, and A. Shirazi-Adl, "A fibril-network reinforced biphasic model of cartilage in unconfined compression," *J. Biomech. Eng.*, vol. 121, pp. 340–347, Mar. 1999.
[34] Y. J. Kim, L. J. Bonassar, and A. J. Grodzinsky, "The role of cartilage streaming potential, fluid flow and pressure in the stimulation of chondrocyte biosynthesis during dynamic loading," *J. Biomech.*, vol. 28, pp. 1055–1066, Sept. 1995.
[35] H. S. Haggerty and H. S. Lusted, "Histological reaction to polyimide films in the cochlea," *Acta Otolaryngol. (Stockh)*, vol. 107, pp. 13–22, 1989.
[36] S. A. Shamma-Donohue, G. A. May, N. E. Cotter, R. L. White, and F. B. Simmons, "Thin film multielectrode arrays for cochlear prothesis," *IEEE Trans. Electron. Dev.*, vol. ED-29, pp. 135–144, 1982.
[37] R. R. Richardson Jr, J. A. Miller, and W. M. Reichert, "Polyimides as biomaterials: Preliminary biocompatibility testing," *Biomaterials*, vol. 14, pp. 627–635, Aug. 1993.
[38] A. M. Dymond, L. E. Kaechele, J. M. Jurist, and P. H. Crandall, "Brain tissue reaction to some chronically implanted metals," *J. Neurosurg.*, vol. 33, pp. 574–580, 1970.

Eric Quenneville was born in Montreal, QC, Canada, in 1975. He received the B.Eng. and M.S. degrees in physical engineering from the Ecole Polytechnique de Montreal in 1999. He is currently working towards the Ph.D. degree at the same university.

In 2000, he joined the Institute of Biomedical Engineering at Ecole Polytechnique de Montreal where his research interests are in the areas of cartilage electromechanics and diagnostic, microfabrication, and thin film processes.

Mr. Quenneville received the best Master Thesis Award, the J. A. DeSeve Foundation Award, the Bechtel Foundation Award, the Labreche-Viger Award, the Canadian Arthritis Network (CAN) Graduate Student Award, and scholarships from NSERC and FCAR between 1998 and 2002 and from the CAN in 2003.

Jean-Sébastien Binette was born in Montréal, Canada, in 1976. He received the B.S. degree in physical engineering and the M.S. degree in biomedical engineering from the École Polytechnique de Montréal, Montréal, QC, Canada, in 2002.

In 1999, he joined the Institute of Biomedical Engineering at École Polytechnique de Montréal to complete the M.S.. He worked to develop a technique to measure cartilage thickness using microelectrodes. In 2003, he joined the Bone and Periodontal Research Centre at McGill University, Montréal, QC, Canada, to work in imaging and biomechanics fields. His research interests are in the area of electrical conductivity of cartilage, imaging, biomechanics, and microelectronics.

Martin Garon was born in 1974. He received the B.Eng. degrees (with honors) in physical engineering from Ecole Polytechnique of Montreal, Montreal, QC, Canada, in 1997. He is currently working toward the Ph.D. degree in the Institute of Biomedical Engineering at Ecole Polytechnique of Montreal.

His research interests include electrode-based medical instrumentation and articular cartilage compositional to functional relationship and electromechanical properties.

Mr. Garon, has received postgraduate scholarships from the Natural Sciences and Engineering Research Council of Canada from 1997 to 2001 and from the Canadian Arthritis Networks in 2002.

Anne Légaré was born in 1973. She received the B.Eng. degree in physics engineering in 1996 and the M.S. degree in biomedical engineering in 1998 from the Ecole Polytechnique de Montreal, Montreal, QC, Canada.

From 1993 to 1995, she was a Research Auxiliary at the Laboratory for the Integration of Sensors and Actuators at the Ecole Polytechnique de Montreal. Since 1999, she is Product Director of the Arthro-BST™, an arthroscopic device for the diagnosis of arthritis, at Biosyntech Canada Inc., Laval, QC, Canada. Her research interests include microelectrode-based bioelectrical signal measurements and analysis, cartilage biochemistry and electromechanics and arthritis-related animal and clinical studies.

Ms. Légaré is a member of the Ordre des Ingénieurs du Québec.

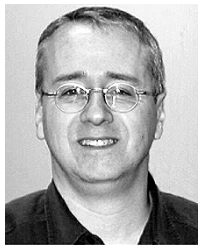

Michel Meunier received the Ph.D. degree from the Massachusetts Institute of Technology (MIT), Cambridge, in 1984.

He is Professor of Engineering Physics at Ecole Polytechnique de Montreal, Montreal, QC, Canada. In the last 24 years, he has been involved in laser and thin film processing of various materials, namely, semiconductors, dielectrics, and metals. He holds a Canadian Research Chair in Laser micro/nano-engineering of materials and he is the director of the Laser Processing Laboratory at Ecole Polytechnique in Montreal. He has published more than 190 papers and is the co-founder of LTRIM technology—a company exploiting new laser processing techniques for microelectronics.

Michael D. Buschmann was born in 1962, received the B.Eng. degree in physics from the University of Saskatchewan, Saskatoon, SK, Canada, in 1984, and the Ph.D. degree in medical engineering and medical physics from the Division of Health Sciences and Technology at the Massachusetts Institute of Technology and Harvard University, Cambridge, MA, in 1992. His postdoctoral training in cartilage microscopy and histology was completed at the University of Bern, Bern, Switzerland, in 1994.

Dr. Buschmann is Professor of Chemical and Biomedical Engineering at Ecole Polytechnique de Montreal, Montreal, QC, Canada and has established a biomedical research program there in fields relating to cartilage and arthritis and a laboratory with expertise in tissue biomechanics, molecular cell biology, multiphoton and environmental scanning electron microscopies, and for the creation of nanostructured biomaterials.